Investigation and Optimization on Effective Parameters of a H-Rotor Darrieus Wind Turbine, Using CFD Method

Mehrpooya, Mehdi*+

Renewable Energies and Environment Department, Faculty of New Sciences and Technologies, University of Tehran, Tehran, I.R. IRAN

Asadbeigi, Mohammad Reza

Hydrogen and fuel cell laboratory, Faculty of New Sciences and Technologies, University of Tehran, Tehran, I.R. IRAN

Ghafoorian, Farzad

Turbomachinery Research Laboratory, Department of Energy Conversion, School of Mechanical Engineering, Iran University of Science and Technology, Tehran, I.R. IRAN

Farajyar, Shayan

Department of Civil Engineering, Science and Research Branch, Islamic Azad University, Tehran, I.R. IRAN

ABSTRACT: *The present study conducted a 2-dimensional numerical simulation using the Computational Fluid Dynamics (CFD) method for a Darrieus Vertical Axis Wind Turbine (VAWT). This study aims to investigate the effect of changing design and operational parameters on the performance of the Darrieus turbine. Power coefficient and torque are calculated to observe the turbine's performance, and their values are compared in the different Tip Speed Ratios (TSR) and azimuth angles, respectively. Therefore, effective parameters such as free wind velocity, chord length, blade number, and airfoil profile are investigated. The results show that increasing the inlet velocity and chord length led to an increase in the efficiency of the turbine and formation of intense wake flow around the blades; however, increasing the number of turbine blades in small TSRs shows better performance, while when the rotor rotations number increases, the low solidity turbine with a lower number of blades has more efficiency. Also, the NACA0021 airfoil profile had higher C_p than other airfoil profiles and augments the wake flow downstream. An optimization method is provided to find the optimal operating and geometric conditions to achieve a higher value of C_p. The results show that the highest efficiency of Darrieus VAWT is achieved with an inlet velocity of 12 (m/s) and blade chord length of 0.2 (m) for a three-bladed turbine at TSR=2.5. It is also shown that Darrieus VAWT operates with lift force and needs an initial torque to start working by increasing the values of C_p in the primary TSRs; the turbine's need for initial torque decreases.*

KEYWORDS: *Vertical axis wind turbine; Darrieus wind turbine; Power coefficient; Wake flow; CFD simulation; Tip speed ratio.*

**To whom correspondence should be addressed.*

+ E-mail: mehrpoya@ut.ac.ir

1021-9986/2023/9/3048-3064 18/$/6.08

INTRODUCTION

Rising concerns about pollution from excessive consumption of fossil fuels have led scientists to research extracting energy from renewable sources. Meanwhile, wind energy was recognized as one of the cleanest renewable energy sources [1]. In order to optimize wind energy and receive the most available energy, wide research was conducted on wind turbines and their types to select the most appropriate kind of wind turbine based on the geographical conditions of the windy region [2]. Also, in some areas, wind turbines are combined with other renewable energy production equipment such as solar panels to create a hybrid power supply system [3]. Wind turbines are classified according to different criteria. One of the most important categories has been based on their rotating axis, which has divided wind turbines into two groups: Vertical Axis Wind Turbine (VAWT) and Horizontal Axis Wind Turbine (HAWT) [4]. HAWTs require a large variety of equipment and components to operate, including a pitch system, a yaw system, a tower, and a strong foundation, which can remarkably increase the cost of building a HAWT [5]. Although the output power of conventional HAWTs is much higher than VAWTs, their complex configuration, expensive control systems and high installation and maintenance cost increased the interest in developing VAWTs [6, 7]. VAWTs, du e to their structure, have capabilities that can produce acceptable power in situations where the HAWTs are not able to work and produce proper power. Operating at high wind speeds and turbulent wind flow are some advantages. In addition, VAWTs are omni-directional and do not require a yaw mechanism[8]. VAWTs perform better in urban environments due to low noise, public safety concerns, and low impact on the environment and have overcome the challenge of the ineffectiveness of HAWTs in low cut-in wind speed and chaotic wind flow in these areas [9]. VAWTs in appropriate sizes can be installed on the roofs of houses; however, the height of the surrounding buildings and the interaction of the atmospheric boundary layer with the different buildings, topography, trees and vegetation of the area should be taken into account because they affect the aerodynamic performance of the turbine [10]. Also this types of turbines can be installed as tidal turbine for power extraction [11]. Furthermore, The use of large generators due to proximity to the ground for large VAWTs does not create design constraints and structural strength challenges, making maintenance, operation, and installation easier [12]. VAWTs are classified into two types, lift-based and drag-based, according to aerodynamic forces. Savonius, which operates by the drag force, has a lower power coefficient and operates at low tip speed ratios but has higher torque, suitable for water pumping [13]. Many design parameters such as buckets arc angle, overlap ratio and number of buckets affect the aerodynamic performance of this type of rotor [14]. The most typical lift-based VAWT used as a source of electricity rather than mechanical power is the Darrieus [15]. This type has no self-starting capability due to symmetrical blade geometry and requires external torque to start [16]. Many parametric studies have been conducted to improve the aerodynamic performance of Darrieus VAWTs and investigate the effects of design and operational parameters such as rotor radius, blade chord length, airfoil profile type, number of blades, wind speed, and flow turbulence model. The examination of each rotor with specific geometric characteristics changes the number of mesh in numerical modeling [17]. Thses studies have been conducted to improve the self-starting and performance of Darrieus turbines. *S.B. Qamar* and *I. Janajreh* [18] studied the effect of solidity and observed that the higher solidity leads to a higher power coefficient in small TSR ranges and improves the self-starting turbine. Furthermore, 3-bladed high-chord turbines attain better performance by reducing the wake behind the turbine and increasing the output torque. Another numerical study has shown that adding winglets help VAWT's self-starting ability significantly and also increases torque and power production by reducing tip vorticities and aerodynamic disturbance [19]. The results of an experimental simulation and two-dimensional CFD study showed that a 3-bladed H-rotor Darrius VAWT with the solidity of 35% had the best self-starting ability[20]. *H.F. Lam* [21] observed that blade tip and span vortices lead to entrainment and turbulence mixing which contributes to wake recovery. This phenomenon causes low torque production of blades at downstream. *M. Ghasemian* [22] investigated the effect of airfoil shape and showed that thicker airfoils are more efficient due to their better stall characteristics. *M.H. Mohamed* [23] studied 20 symmetric and non-symmetric airfoils and showed that S-1046 non-symmetric airfoil increased relative Cp by 26.83% compare to NACA airfoils. Also, the results obtained from a numerical study that was conducted

on different symmetric and asymmetric airfoil profiles showed that the LS(1)-0413 airfoil profile had the best C_p and the NACA 63-415 airfoil profile had the best operating range [24]. By changing the geometry of the airfoil and applying cavity layouts near the leading or trailing edge due to more effective flow control on the blades, the efficiency of the Darrieus turbine was improved [25]. *I. Paraschivoiu* [26] used variable pitch control to gain a 27% relative increase in efficiency and better performance at low tip speed ratios. Inlet wind speed is one of the parameters affecting the performance of wind turbines, and the results showed that with increasing inlet wind speed, wind turbine power coefficient has also increased [27, 28]. Increasing this parameter on C_p was more evident in low TSRs [29]. Another effective parameter is the aspect ratio, which is the relation between rotor diameter and height (H/D). The results show that in the initial TSRs, C_p rose with an increasing aspect ratio[30]. Three-dimensional results indicated that larger blades enhanced VAWT performance also, the presence of end plates with appropriate size improved H-type Darrieus VAWT performance [31]. Twisted blades were also a new method for Darrieus turbines, and converting the H-rotor turbine into a helical turbine increased efficiency and reduced rotor vibrations [32]. Also, the effect of different turbulence models on an innovative H-type Darrius VAWT with auxiliary blades was studied and the results showed that the Spalart-Allmaras turbulence model performs better in low TSRs; however, the k-ω turbulence model in high TSRs has higher efficiency [33]. Another operating condition affecting the performance of H-type Darrius VAWT is the angle of attack. The effect of the angle of attack on a specific airfoil profile showed that the angle of attack from 0° to 12° leads to a wider jet frountier, while the trend is reversed from the angle of attack from 12° to 25° [34]. Furthermore, the higher jet flow velocity led to a smoother velocity profile around the blades, and also the higher jet flow velocity led to a weaker wake flow around the blade airfoil profile [35]. Flow controlling by co-flow jet's airfoil had results in separation delay which increased the lift to drag ratio of airfoil [36]. The effect of helical angle and pitch angle, which affects the angle of attack and subsequently Cp values, was evaluated and the results showed that a pitch angle of -2° and a helical angle of 0° had the highest efficiency [37]. Various methods have been adopted to analyze the performance of wind turbines. The MST method is another approach for the aerodynamic analysis of VAWTs. This method has been used to study the giant Sandia turbine[38]. The DMST method, which is more precise than the MST method, has been used to analyze the flow around VAWTs [39]. This method is used to study the design and aerodynamic parameters of a Gorlov VAWT [40]. A numerical analysis method with the help of QBlade commercial software has been performed on different types of wind turbines and the data is based on Xfoil numerical information [41]. Although the Qblade solution method and the DMST use potential solution, since the DMST data is derived from experimental results, it is more accurate than the Qblade adopted from Xfoil [42]. The most promising methods of numerical solution is a simulation based on Computational Fluid Dynamics (CFD) which is discretization of the Navier-Stokes equation. The CFD method is more accurate than the computational aerodynamics methods, which include a series of assumptions and simplifications in this model [43]. The CFD method has been used for various applications like numerical analysis of flow water [44]. Different methods can be used for CFD simulation, the 1D CFD solution is one of them which reduces the computational time [45]. The two-dimensional solution of CFD shows a better view of complex vortices, and prediction of dynamic stall than BEM method [46]. The 2D CFD method was studied to compare two different VAWTs with various geometries and operating conditions and the effect of wind speed on its aerodynamic behavior [17]. A precise 3D CFD solution has been performed to investigate the secondary flows and tip effects, and it has been observed that the 2D solution predicts more power due to reduced turbine performance by creating a vortexat the blade tips [47]. Various methods have been employed to optimize VAWTs. The Genetic algorithms was used to optimize the aerodynamics of the airfoil of a Darrieus turbine in different TSRs and the performance increase of 26.82% was achieved in the moderate TSR[48]. Another way of optimization was the DOE method. This method was adopted to find the optimal airfoil profile using control points for a Darrieus VAWT and it was shown that the most suitable airfoil increases power generation by 28%[49]. The benefit DOE method is to prepare a systematic way for verifying the analytical results with more time effectiveness. In addition, it can be more robust in estimating each parameter and understanding the interactions between

Table 1: Dimensions and main geometric characteristics of the simulated turbine rotor and stator

	Quantity	Value
1	Number of blade	3
2	Profile of blade	NACA0021
3	Length of chord	0.0858(m)
4	Radius of rotor	0.515(m)
5	Height of blade	1(2D simulation)
6	Length of stator	25(m)
7	Width of stator	4(m)

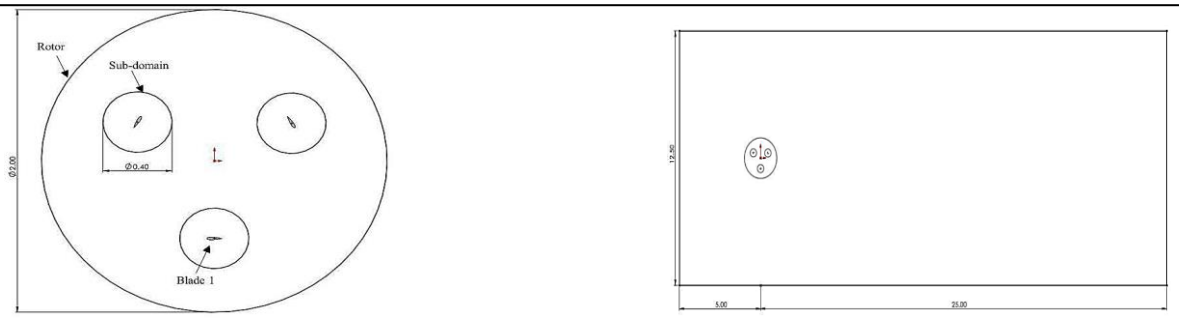

Fig 1: a) Schematic of the 3-bladed darrieus turbine with dimensions. b) schematic of the stator with dimensions

them [50]. Sensitivity analysis, which is an important step in the analysis of wind turbines, has been performed between design parameters such as solidity, rotor diameter, airfoil shape and wind velocity[51]. The Kriging method is a widely used and accurate alternative model for response surface analysis. The relationship (response surface model) between the optimization objective (the highest value of power factor) and the design and operating parameters can be precisely defined based on the Kriging model [52]. *M. H. Ranjbar* utilized the Kriging method to find optimal duct angles to maximize velocity in the throat [53].

In this study, a numerical analysis of the effect of various parameters, namely wind velocity, blade chord length, airfoil profile, and blade number, has been investigated on the efficiency, aerodynamic performance and self-starting ability of a H-rotor Darrieus VAWT. The novelty of this study is finding the optimal turbine geometry and operating conditions based on the conducted parametric CFD study in order to generate maximum power. Therefore, by adapting an appropriate optimization model, this aim will be achieved. Also, a brief insight into the self-starting ability which is a crucial issue in the Darrieus turbine has been provided.. Thus, the 2D-CFD simulation, suitable for H-type Darrieus VAWTs, has been performed. The analysis is conducted by commercial software, ANSYS Fluent and finally, by adopting the Kriging method, an optimized geometry was selected with the highest efficiency.

THEORETICAL SECTION

Problem description and solution strategy

In this numerical 2D study, a Darrieus VAWT was considered as a prototype. The aerodynamics of this turbine were studied; therefore, the arms and shafts were omitted. All blade profiles inside the Rotor sub-domain area of 0.4(m) diameter were enclosed in a control circle. Unlike the interface, it does not have any physical significance. It aimed to prepare an accurate dimensional control of the grid elements around rotor blades. Also, a rectangular is considered as the stator. The geometric features of the rotor and stator considered by *M. Raciti Castelli et al*. [54] are summarized in Table 1.

The geometry of the rotor and stator is shown in Fig 1, and the dimensions and characteristics of turbine and stator are given in Table 1.

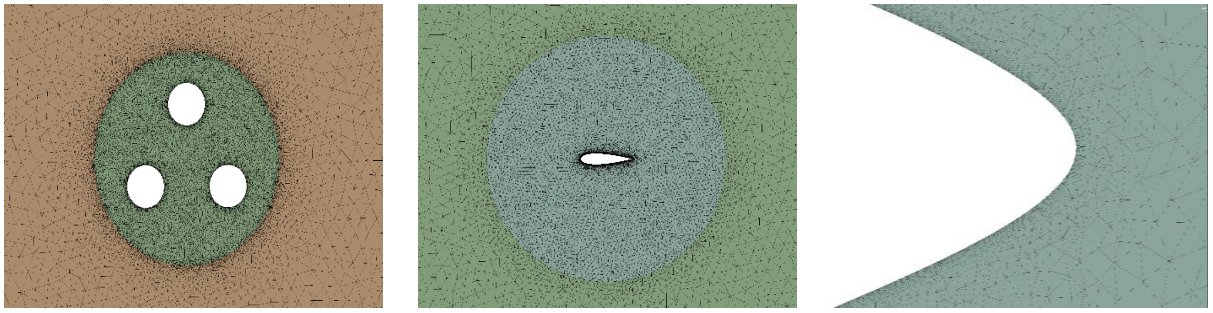

a *b* *c*

Fig 2: a) Rotor mesh, b) Sub-domain mesh and c) Airfoil boundary layers and mesh

In this simulation, an unstructured grid was chosen, and the mesh motion approach was adopted to simulate the rotor motion. Also, the all triangles method was used for the rotor and stator domains. To improve the CFD results, the rotor and stator interface as well as the sub-domain and rotor interface, are proportionally sized. Also, for more precise CFD results and to capture the effects of flow separation around the blades, especiwally near the leading and trailing edge, a suitable grid size and boundary layer mesh, which contains 10 layers with a growth factor of 1.1, were adopted. Mesh is shown in Fig 2.

Governing equations

In this CFD analysis, the Navier-Stokes equation simulates the flow around the Darrieus turbine rotor, Reynolds averaging is used, and the velocity is divided into two terms, $\bar{u}$ and u′, which are averaged and the fluctuating velocity. Also, equations 3 and 4 represent the Unsteady Reynolds Average Navier Stokes (URANS) [55].

$$\overline{u} = \frac{1}{T}\int_T u(t)dt \text{[55]} \quad (1)$$

$$u' = u - \overline{u} \text{ [55]} \quad (2)$$

$$\frac{\partial \overline{u_i}}{\partial x_i} = 0 \text{ [55]} \quad (3)$$

$$\frac{\partial \overline{u_i}}{\partial t} + \overline{u_j}\frac{\partial u_i}{\partial x_j} = -\frac{1}{\rho}\frac{\partial \overline{p}}{\partial x_i} + \nu\frac{\partial^2 \overline{u_i}}{\partial^2 x_j^2} - \overline{u_j'\frac{\partial u_i'}{\partial x_j}} \text{ [55]} \quad (4)$$

Where u is the velocity of fluid flow (m/s) in the x-direction, p is pressure (Pa), and ρ (kg/m^3) is the fluid density.

Choosing the Turbulence model is crucial due to flow separation and great pressure gradient, which remarkably impact CFD results. Several commonly used turbulence models include k-ε, k-ω, and SST transition. These models use the Boussinesq assumption shown in Equation (5) for Reynolds stresses [56].

$$\tau_{ij} = 2\mu_t\left(S_{ij} - \frac{1}{3}\frac{\partial u_k}{\partial x_k}\delta_{ij}\right) - \frac{2}{3}\rho k\delta_{ij} \quad \text{[56]} \quad (5)$$

$$S_{ij} = \frac{1}{2}\left(\frac{\partial u_i}{\partial x_j} + \frac{\partial u_j}{\partial x_i}\right)\text{[56]} \quad (6)$$

The k-ω SST model was used because this model can reduce computational costs. Also, this approach is widely used for modeling the flow around turbomachines; also, the k-ω SST equations for applications near wall regions are suitable [57]. These models are based on transport equations for the turbulence kinetic energy, *k*, and its dissipation rate ω. It is a two-equation model, which includes two extra transport equations to represent the turbulent properties of the flow. This allows a two-equation model to account for history effects like convection and diffusion of turbulent energy. The model uses the following transport equations:

$$\frac{Dk}{Dt} = P - \beta^* \rho\omega k + \frac{\partial}{\partial x_j}\left[\left(\mu + \sigma_k\frac{\rho k}{\omega}\right)\frac{\partial k}{\partial x_j}\right] \text{[56]} \quad (7)$$

$$\frac{D\omega}{Dt} = \frac{\gamma\omega}{k}P - \beta\rho\omega^2 + \frac{\partial}{\partial x_j}\left[\left(\mu + \sigma_\omega\frac{\rho k}{\omega}\right)\frac{\partial \omega}{\partial x_j}\right]\text{[56]} \quad (8)$$

The ω determines the scale of the turbulence, whereas, *k*, determines the energy in the turbulence.

$$P = \tau_{ij}\frac{\partial u_i}{\partial x_j}\text{[56]} \quad (9)$$

Where P is turbulence-energy production and τ_{ij}derived from Equations (5) and (6).

The turbulent viscosity is assumed from the below equation:

Table 2: Constants of model k-ω [58]

C_μ	σ_k	σ_ω	β^*	β	γ
0.9	0.5	0.5	0.09	0.072	0.52

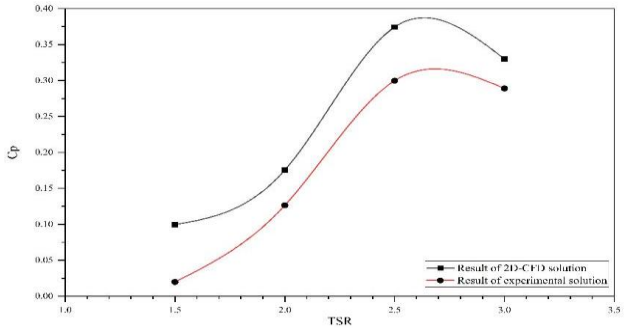

Fig 3: C_P values from CFD simulation compared with the experimental study results

$$\mu_t = \frac{\rho k}{\omega}[56] \quad (10)$$

The other parameters of the above equation are obtained from Table 2.

The γ coefficient was selected to obtain the appropriate value for the von Karmen constant (κ ≈ 0.41), *via* the Expression (11):

$$\gamma = \frac{\beta}{\beta^*} - \frac{\sigma_\omega k^2}{\sqrt{\beta^*}}[56] \quad (11)$$

The tip speed ratio is the ratio between the blade tip speed and the wind speed (V_w). [55].

$$TSR = \frac{R \times \omega}{V_{in}}[55] \quad (12)$$

Where R is the radius and ω is the angular velocity of the rotor.

The power coefficient (C_p), which is the relation between the product of rotor torque and angular velocity with wind power, can be written as follows:

$$C_P = \frac{P}{\frac{1}{2}\rho A V_{in}^3}[59] \quad (13)$$

Where ρ (kg/m^3) wind densities, V_{in} (m/s) is wind speeds entering the turbine, T (N.m) is turbine torque, P (W) is the extractable power, and A (m^2) is the swept area.

The aerodynamic performance and operating TSR range of turbine highly depends on solidity, was defined as:

$$\sigma = nc/R\ [42] \quad (14)$$

Which n is the number of blades, and c is the blade chord length.

Numerical modeling and simulation

Boundary condition

For this 2D-CFD simulation, the unsteady Reynolds-averaged Navier-Stokes (URANS) commercial solver Ansys Fluent v. 21 was chosen. Due to interactions between the blade's movement and the wake flow and the unsteady nature of the problem, the transient approach was performed. The inlet of the stator (left side of domain in Fig 1b) is defined as the boundary condition of the velocity inlet. The stator outlet (right side of the domain in Fig 1b) is considered the pressure outlet. The sides of the stator are set as symmetry. The rotor interface is appropriately coupled to the stator interface by sliding mesh approach, and the interfaces of sub-domains are coupled with the rotor. In this numerical study SIMPLE scheme is adopted, and second order upwind spatial discretization was obtained for pressure, momentum, and turbulence equations. Also, the absolute convergence criteria for residuals were set to 10^{-6}. Also, the global CPU time was approximately about 4-5h for converging.

Validation and grid independence

The experimental study of a 3-bladed Darrieus turbine conducted by *Castelli et al*. [54] was selected. The inlet velocity of 9(m/s) was adopted in a wind tunnel to carry out the experimental test. The output numerical results were compared to experimental study data at 4 different TSRs to verify the current 2D-CFD study. The validation results for C_p are shown in Fig 3.

As shown in Fig 3, the numerical simulation results had an acceptable agreement with the experimental study results; therefore, the method of numerical analysis is reliable. The maximum and minimum C_p error is related to the λ=1.5 and λ=3 with 380% and 12% error, respectively. At λ=1.5, the experimental turbine power is close to zero however, the 2D simulation predicts a slightly higher value. The cause of the difference in 2D numerical simulation is due to the lack of prediction of blade tip vortices and ignorance of turbine arms and rods in simulation.

In the next step, the grid independence was performed; thus, the mesh around the 3 sub-domains, rotor domain,

Table 3: Grid independence analysis

	Case	C_p value
1	Case 1	0.175
2	Case 2	0.201
3	Case 3	0.192

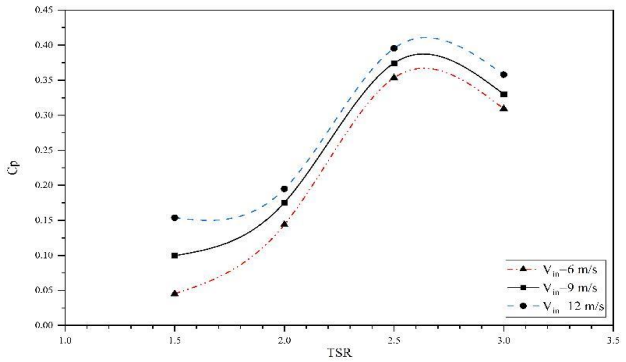

Fig 4: Effect of free wind velocity on C_p

and airfoil profiles which significantly impacted the results, was gradually made smaller, and the C_p at TSR=2. Three different cases were considered to study grid independence. The total number of grids in the first, second and third cases was 255000, 370000, and 570000, respectively. C_p values at TSR=2 are given in Table 3.

As shown in Table 3, the C_p values are not significantly different in four cases. The C_p value of the second and third case is 12% and 9% higher than the first case. As a result, the numerical solution does not depend on the number of grids. Case 1 has obtained more accurate results with a lower mesh number. Therefore, for lowering computational time, Case 1 was selected for the following simulation

RESULTS AND DISCUSSION

In this section, based on the effectivity of free wind velocity, blade chord length, blade number, and blade airfoil profile on the efficiency of wind turbines, mentioned parameters are numerically analyzed.

Effect of free wind velocity

The effect of V_{in} on the C_p of H-type Darrieus VAWT is inspected for variousTSR values with the inlet velocity range from 6(m/s) to 12(m/s). The blades Reynolds number are 35k, 53K and 70k corresponding to inlet velocity of 6, 9 and 12 (m/s). The results are illustrated in Fig 4.

As the results show, the C_p value is negligible in small TSR values in all cases, so an initial torque is required to start the turbine. Also, the C_p values increase with mounting free wind velocity; in other words, the turbine output power increases with rising free wind velocity. Notably, the growth rate of C_p in small TSR values was more than in large TSR values. Finally, the highest value of power coefficient was equal to 0.4, which occurred in V_{in} = 12(m/s) and TSR = 2.5. For a better understanding, the velocity contour plots for the three free wind velocities are shown at TSR=2.5 in Fig 5.

According to the contours, the wake flow in the downstream area of the turbine rotor was much stronger and longer when the free wind velocity was 12(m/s) compared to when its velocity value was 6(m/s) and 9(m/s) which is indicating the more wind energy extraction. Also, when the free wind velocity is high, the unfavorable pressure gradient upstream of the turbine rotor is reduced, which intensifies in the downstream zone wake flow. Obviously, by increasing the free wind velocity value, the flow velocity passing through the upper and lower areas of the turbine rotor has increased and subsequently leads to an increase in torque values in this condition. Also, the turbine torque was plotted as a function of azimuth angle at TSR = 2.5 to show the rotor torque in a rotation. The results are shown in Fig 6.

The results showed that free wind velocity increased rotor torque at each azimuth angle. Also, TSR = 2.5 and V_{in}=12 m/s, which is the highest torque value, indicate the maximum output power in this condition. However, it should be noted that the increase in free wind velocity, which helps Reynolds number growth, could not significantly increase torque and C_p value.

Effect of blade chord length

In this part, the impact of blade chord length on the turbine performance was evaluated, and values of 0.085 (m), 0.15 (m), and 0.2 (m) were considered as blade chord length. Fig 7 shows the C_p vs. TSR.

As it is clear from the results, the amount of C_p has increased remarkably with increasing the chord length. The maximum value of C_p is obtained at TSR=2.5, around 0.55, corresponding to the chord length of 0.2(m). The C_p value of blade chord length of 0.15(m) and 0.2(m) increased about 37% and 57%, respectively. Also, with growing blade chord length, turbine solidity increased;

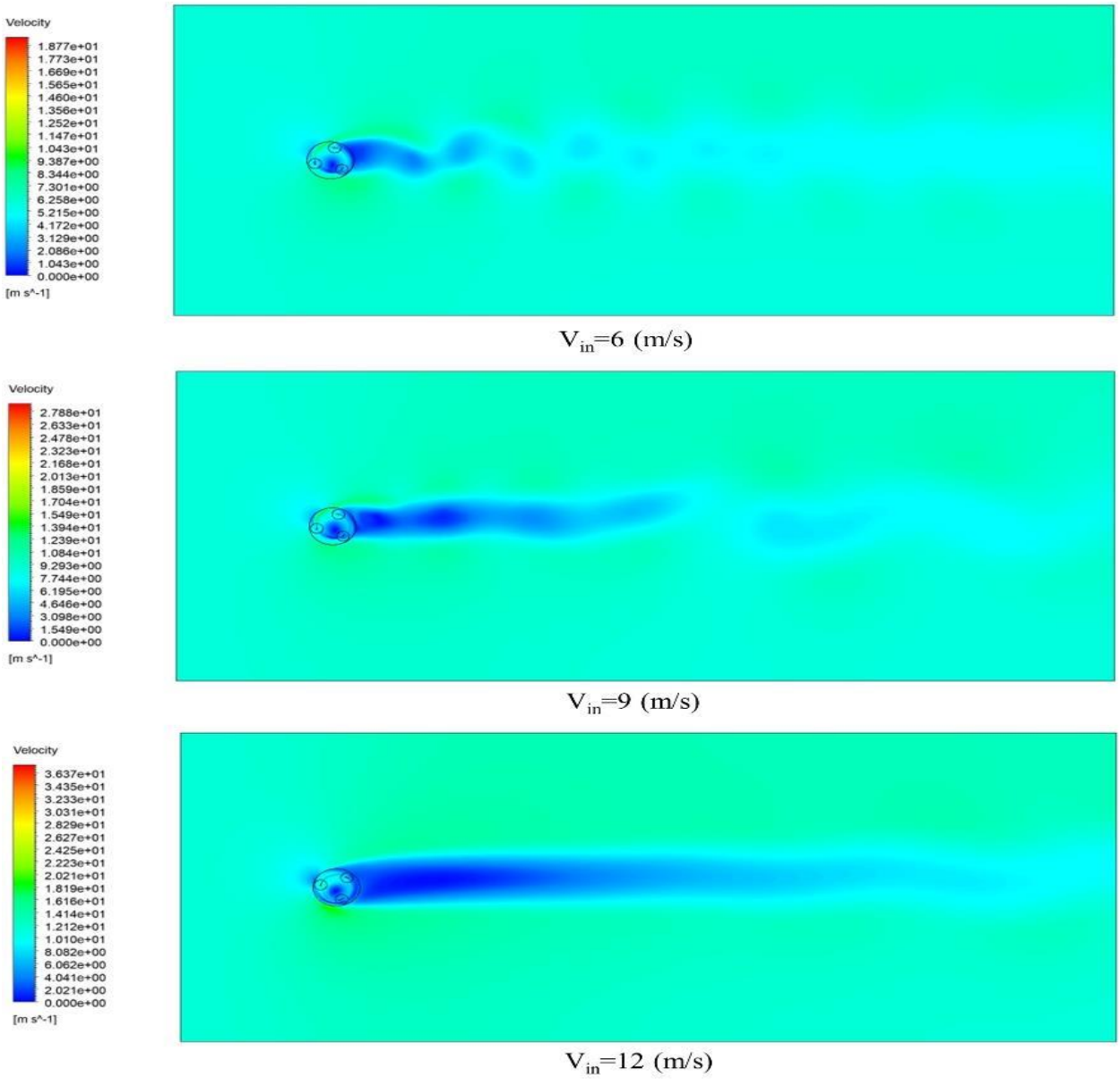

Fig :5 Velocity contour plots for rotor with varying free wind velocity at TSR=2.5

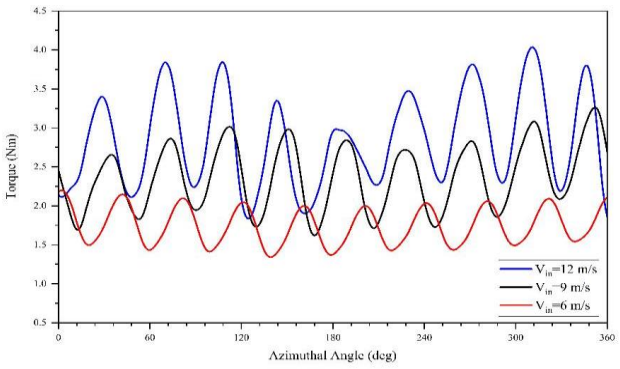

Fig 6: Torque plot for different free wind velocities at TSR 2.5

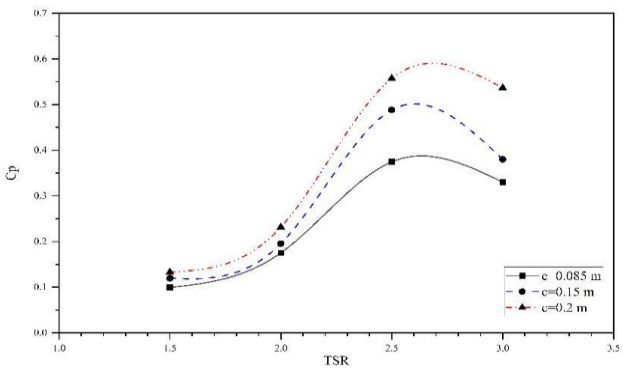

Fig 7: C_P values for different blade chord lengths

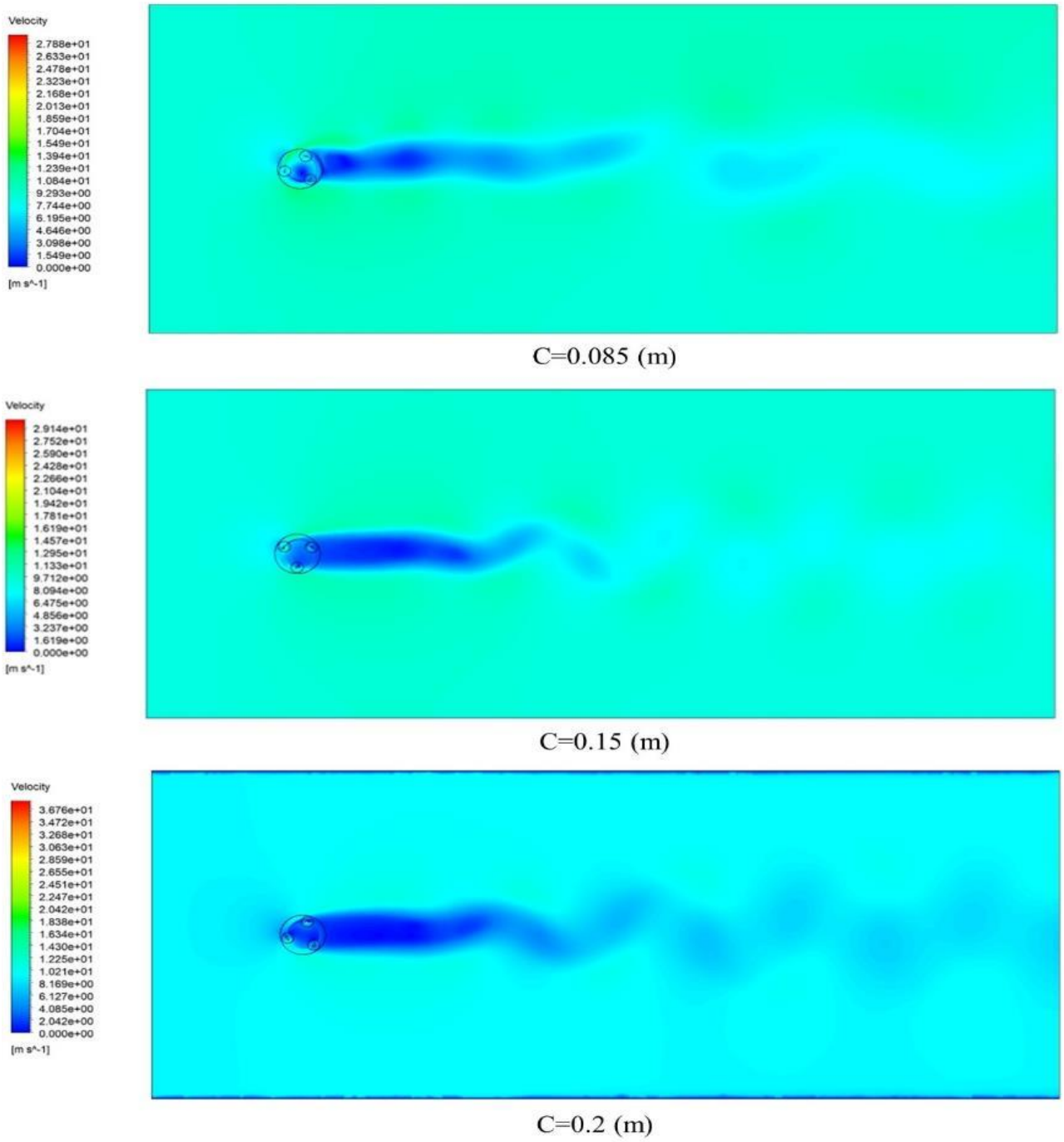

Fig 8: Velocity contour plots for rotors with different chord lengths at TSR=2.5

thus, wind flow involved a larger cross-section of the turbine blades, resulting in higher wind turbine efficiency. Also, velocity contour diagrams for the three diverse structures of various blade chord length are illustrated at TSR=2.5 in Fig 8.

From the above contour plots and their widespread wake flow, the significant solidity impact prompted by the substituting in blade chord length was clearly observed. Pertaining that the turbine solidity raises by the blade chord length, the downstream wake zone of the turbine becomes more extreme in making an extended and low-velocity wake flow because the rotor obstructed much of

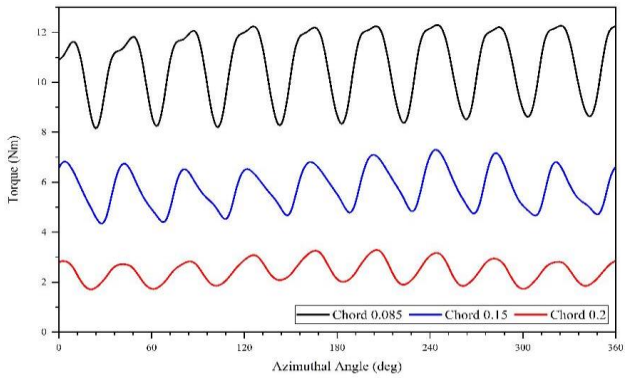

Fig 9: Torque plot for different blade chord lengths at TSR 2.5

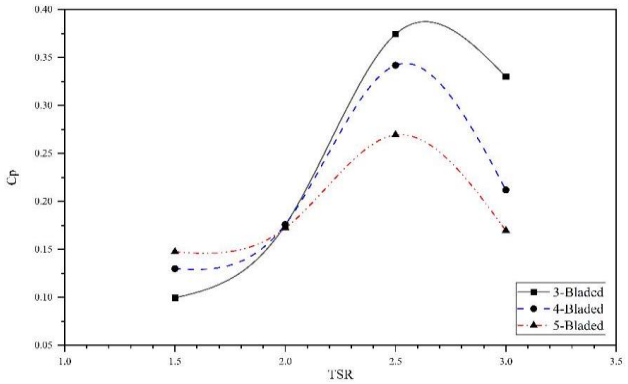

Fig 10: C_p values for different blade number

the incoming wind stream. As a result, the formed wake flow at the turbine upstream causes a lack of access of the blade at downstream to the clear flow which reduces blade torque production in this region. This causes the front section of the rotor to be more near-stagnation than the rotors with lower solidity. This condition decreases the wind velocity and creates an unfavorable pressure gradient growth at upstream, which contributes to a noticeable wake flow formation right behind the rotor. However, this wake flow caused a more intense favorable pressure gradient upstream and downstream of the rotor, which increased the airflow velocity on the rotor and resulted in a higher axial velocity and higher C_p for the high-solidity turbine. Also, Fig 9 illustrates the turbine torque as a function of azimuth angle, and its graph was plotted at TSR = 2.5.

A turbine with a higher chord length and solidity produces more torque. This condition indicates greater extractable power and lower initial torque value to operate a turbine.

Effect number of blades

In this chapter, the influence of blade number on the turbine performance was studied for a turbine with 3, 4, and 5 blades. The results of the C_p value for different blade number are shown in Fig 10.

Regarding the details of Fig 10 in small TSRs, the C_p values for five-bladed and four-bladed turbines were 67% and 44% higher than three-bladed turbines, respectively, and helped turbine self-starting. Also, the increasing trend stopped at higher TSRs, and the three-bladed turbine showed better performance. The C_p values of five and four blades' turbines were 27% and 8% lower than the C_p values of the 3-bladed turbine at TSR=2.5. Velocity contour diagrams for rotors configuration with different blade number at TSR=2.5 are shown in Fig 11.

The results obtained from Fig 11 showed that the number of turbine blades significantly affects its solidity and the wake flow generated at downstream of the turbine. This is due to the turbine with a higher blade number in high rotational speed creating intensive vortices and wake regime within the rotor, resulting in significant power generation reduction. However, its effect is generally different from changing blade chord length effect. The rotor with higher solidity impeded the incoming flow; therefore, it stretched the frontal stagnation area forward. In other words, it developed an unpleasant pressure gradient whereas it caused acutely dispersing incoming flow onto the sides of the rotor, which caused a favorable pressure gradient. It should be noted that the intense wake region in the space between the turbine blades and high produced side velocity due to the solidity can weaken the four and five-bladed rotor performance in higher TSR values. The turbine torque as a function of azimuth angle was plotted in Fig 12 at TSR = 2.5.

The four-bladed and five-bladed rotors underwent low and fluctuating treatment among a thorough turbine rotation at TSR=2.5. These intensive fluctuations and low torque values related to four and five-bladed turbines are attributed to more blade to blade interaction, and the single blade wake region, remained between rotor blades, diminishing the function of the second blade; as a result, torque and also C_p values decreased remarkably in high TSR values.

Effect of airfoil profile

To discuss the influence of the blade airfoil profile on the turbine performance, The numerical modeling was carried out for three symmetrical airfoils, namely NACA 0015, NACA 0018, and NACA 0021, and the output data for C_p values of mentioned airfoil profiles at varying TSRs are shown in Fig 13.

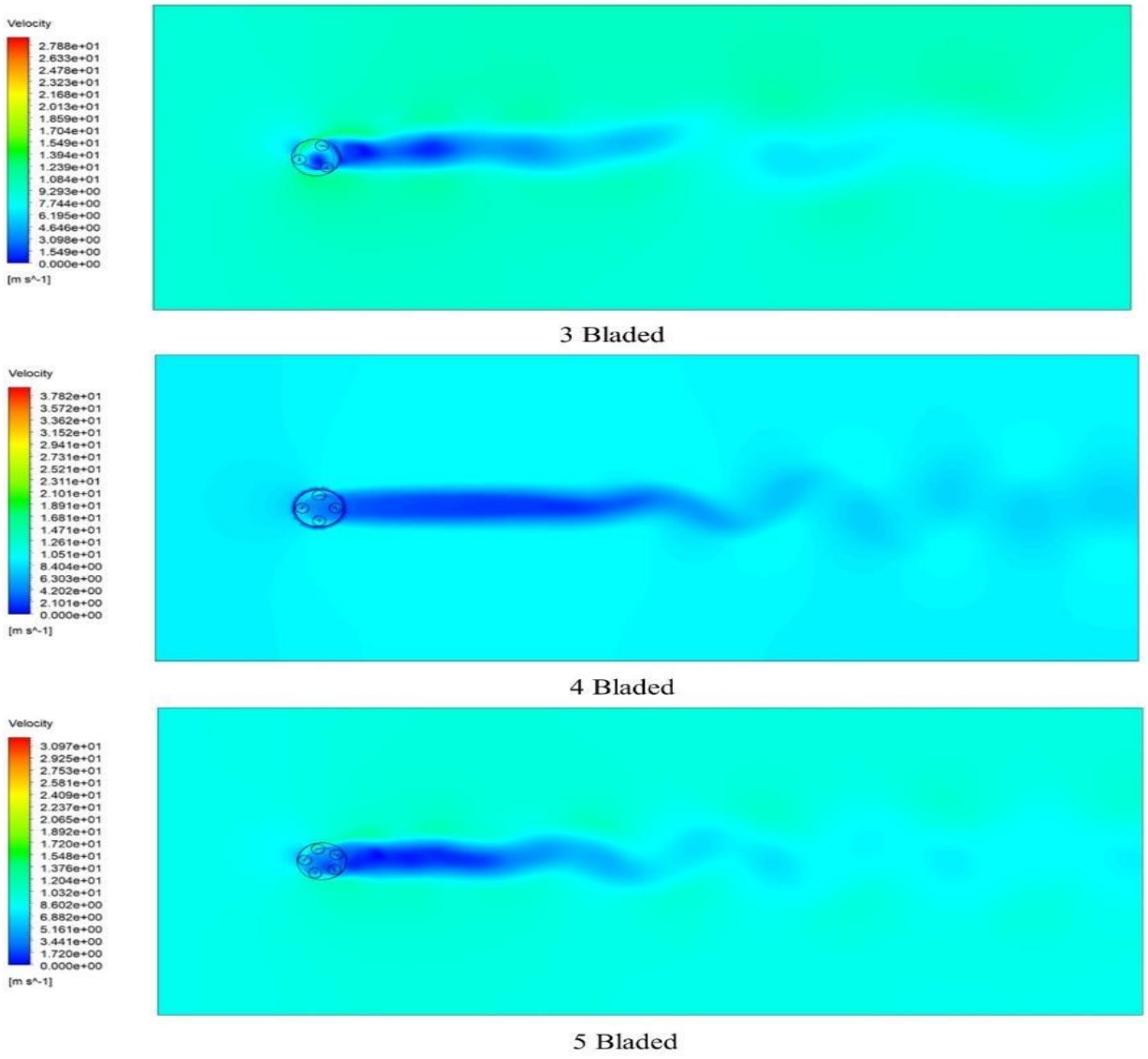

Fig 11: Velocity contour plots for rotors with the varying number of blades at TSR=2.5

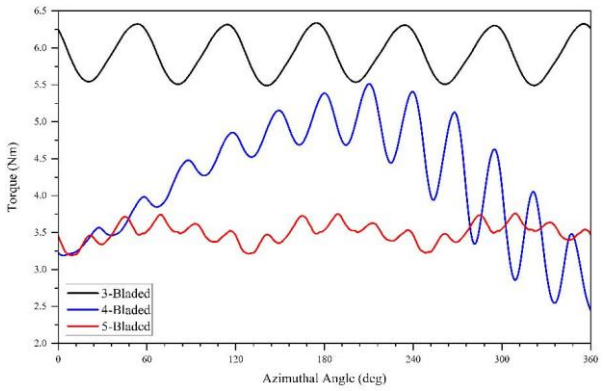

Fig 12: Torque plot for different blade number at TSR 2.5

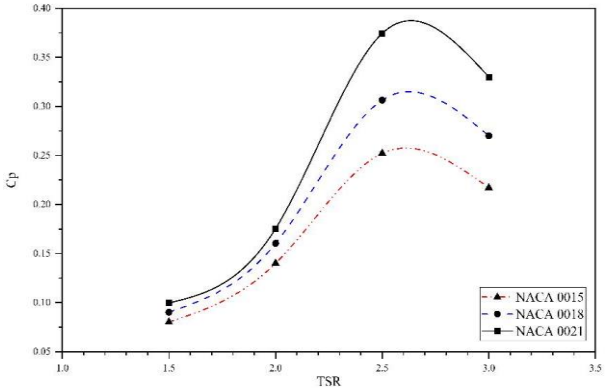

Fig 13 :C_P Values for different NACA airfoil profiles

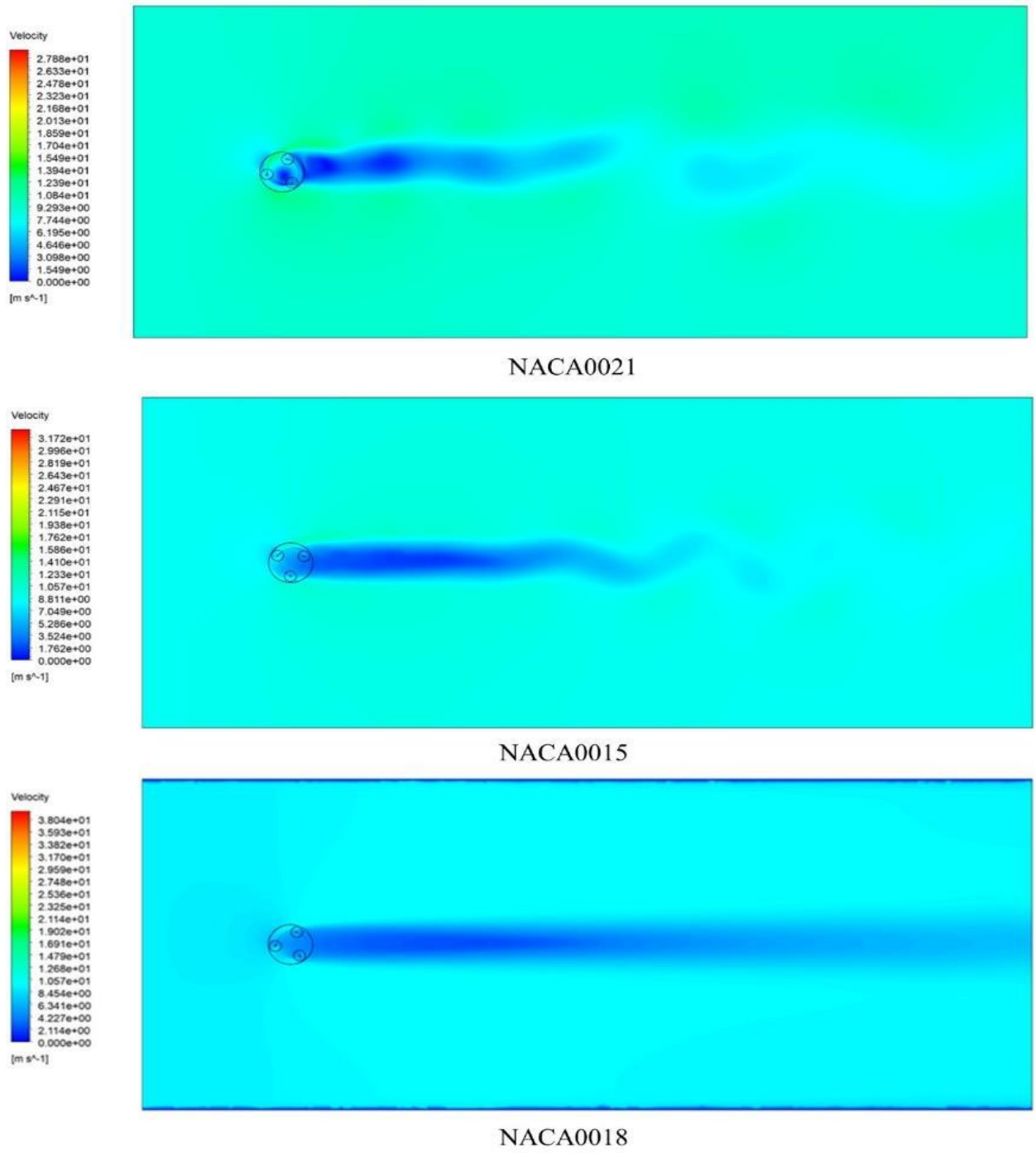

Fig 14: Velocity contour plots for rotors with different blade airfoil at TSR=2.5

The results showed that the performance of the Darrieus turbine was maximum when the NACA 0021 airfoil profile was selected for the design and the maximum C_p value of the NACA 0021 airfoil at TSR=2.5 is 19% and 32% higher than the NACA 0018 and NACA 0015 airfoil profiles, respectively. As a result, due to the larger amount of C_p associated with the NACA 0021 airfoil profile in small TSRs, less initial torque is required for the initial rotation of the rotor, and it is more suitable for design. Also, velocity contour plots for various rotor blade airfoil profiles at TSR=2.5 are shown in Fig 14.

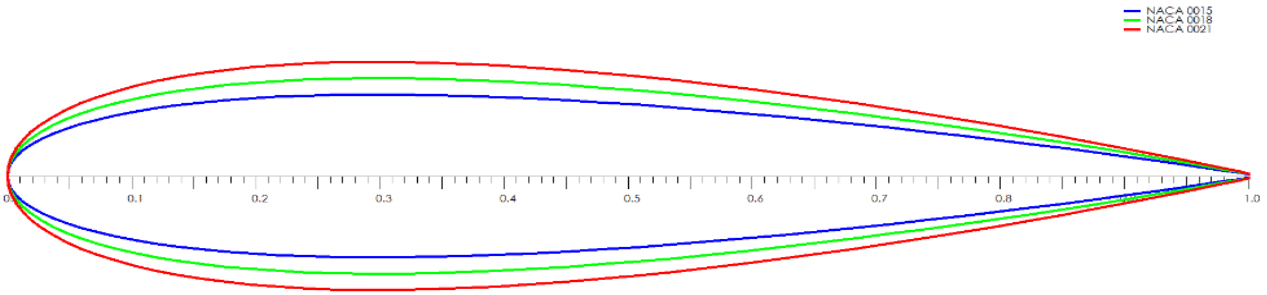

Fig 15: Comparison of various NACA airfoils employed with their thickness

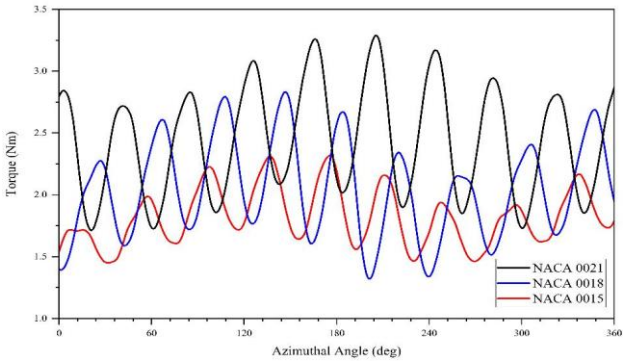

Fig 16: Torque plot for different NACA airfoil profiles TSR 2.5

Regarding contour plots, in the turbine with NACA0018 and NACA0015 configuration, an intense wake region dispersed significantly between rotor blades, and a negative pressure gradient can also be sensible in front of the rotor with NACA0018 design, which led to a decline in C_p value. Another critical point is that the thickness of the NACA0021 airfoil profile is greater than the other two airfoil profiles, which have shown in Fig 15; therefore, the flow streamlines are in contact with a larger cross-section and end up reducing the unfavorable vortex trapped at the trailing edge of the airfoil and increasing efficiency. However, higher blade thickness in high TSRs forms a strong wake around the blades, causing a C_p drop.

As can be seen from Fig 16, all three rotors with different configurations have experienced severe oscillations in one rotation. Also, the rotor designed with the NACA0021 airfoil profile had the highest maximum torque during a complete rotation; however, this difference in the amount of torque was not significant.

Optimization

For the optimization process, the design of experiments approach (DOE) was applied as a methodology to investigate the impacts of different design and operating parameters that were discussed in the previous section. The main goal of the DOE approach is to choose each geometrical parameter to define the shape design space well. Considering the rather insignificant number of control points, a factorial method is suitable for this approach[49]. For optimization with these methods, there are different optimization techniques namely Mixture design, Taguchi, and Response Surface Methodology (RSC), the first method is for the formulation, the second solution is for process conditions, and the third one has simultaneous application for both process and formulation changes [60]. Since the experiment steps were pre-designed and the effects of various parameters were investigated, the DOE method was set to custom mode. In the response surface section, different methods were examined. According to the observation of the existing errors, the Kriging method with variable Kernel variation type was the most optimal and accurate mode.

Figs 17 to 19 are shown the results of the response surface in different conditions based on Kriging method.

According to the above diagrams, the best power coefficient was illustrated at about 0.58. The sensitivity coefficient of the parameters was obtained, and that is shown in Fig 20.

According to Fig 20, the TSR value had the highest, and inlet velocity had an almost negligible sensitivity on the power coefficient of the turbine at 38.19% and 11.2%, respectively. Among four influential factors discussed previously, this issue proved that blade chord length was the most impressive factor. In other meaning sensitivity of this factor is approximately 19.36%.

Finally, the optimal operating conditions were determined after the optimization process with the mentioned method, which is given in Table 5.

Table 4: Goodness of fit

Model	Coefficient of Determination	Root Mean Square Error
Kriging	1	5.4758e-9

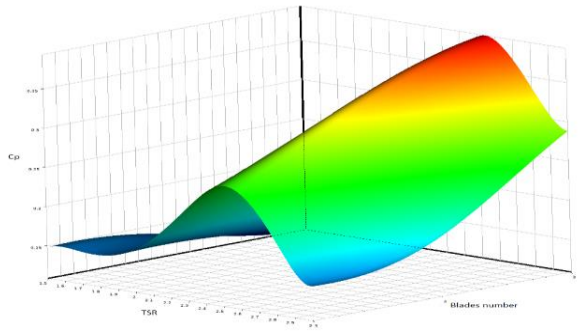

Fig 17: C_p based on TSR and different blade number

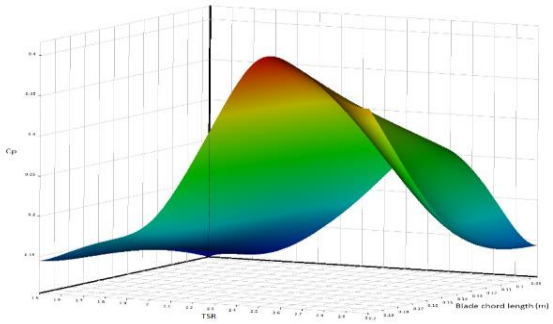

Fig 18: C_p based on TSR and different chord length

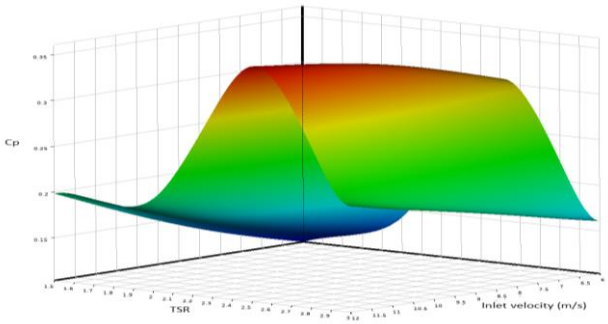

Fig 19: C_p based on TSR and different inlet velocities

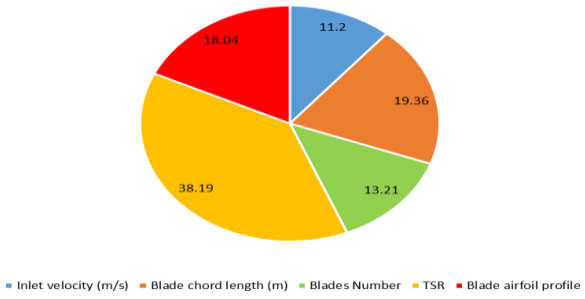

Fig 20: Local sensitivity

Table 5: Operating conditions of the optimal geometry

	Quantity	Value
1	Chord Length	0.2 (m)
2	Velocity Inlet	12 (m/s)
3	TSR	2.5
4	Airfoil Profiles	NACA0021
5	Blade Number	3

CONCLUSIONS

In this study, a numerical simulation based on the CFD method was performed for the aerodynamic design of Darrieus VAWT using ANSYS Fluent software. A 2D rotor is considered to represent a severed section of the 3D rotor, separated into three areas namely stator, which was the stationary zone, the rotor domain, which was considered as rotating area, and sub-domains which were around the airfoils and their rotating were dependent on the rotor. The results showed that with increasing wind speed, which also leads to an increase in Reynolds number, C_p has risen continuously. It is noteworthy that the effect of increasing the value of the inlet wind velocity on increasing the C_p at low TSR values was more significant. Also, the study on the blade chord length showed that higher values of this parameter improved the turbine performance at all TSR values , and by increasing the chord length, initial turbine torque was boosted. By adding blade number, the solidity can be increased, and relevantly larger C_p values are gained in low TSRs. Moreover, less initial torque is required to begin rotation. However, with increasing TSR values, the turbine with fewer blades was more efficient. At the maximum TSR value, the torque of the 3-bladed turbine in a complete cycle was higher than other configurations. Also, the effect of the blade to blade interaction and the number of blades on the wake flow intensity in rotor downstream zone and in the space between the turbine blades shows that although the number of blades increases solidity like blade chord length, the effect of blade number was different with chord length. It means that increasing the number of rotor blades does not have a steady upward trend like increasing the blade chord length for C_p value as a function of TSR. The investigation of the airfoil profile showed that the highest torque and C_p values were obtained for the turbine with the NACA0021 airfoil profile due to its higher thickness. It is notable that, an augment in blade chord length, number of blades, and blade thickness contributes to wake flow formation, especially in high rotational speed. Finally, the Kriging optimization model suggests that 3-bladed turbine with c=0.2 (m), NACA 0021 airfoil and

V_{in}=12 (m/s) operating at TSR=2.5, will attain the maximum C_p value.

Nomenclature

Symbols

V_{in}	Inlet flow velocity (m/s)
T	Torque (N.m)
P	Output power (W)
R	Rotor radius (m)
A	Swept Area (m^2)
C_p	Power coefficient
C_m	Torque coefficient
c	Blade chord (m)
n	Number of blades

Greek

μ	Viscosity (Pa.s)
ω	Angular velocity (rad/s)
ρ	Density (kg/m^3)
σ	Solidity

Subscript

t	Turbulence
w	Free wind flow

Abbreviations

VAWT	Vertical axis wind turbine
HAWT	Horizontal axis wind turbine
CFD	Computational fluid dynamic
DMST	Double multi-stream tube
MST	Multi-stream tube
URANS	Unsteady Reynolds averaged Naive Stokes
TSR	Tip speed ratio
DOE	Design of experiments

Received : Now. 24, 2022 ; Accepted : Jan. 21, 2023

REFERENCES

[1] Dixon S.L., Hall C.A., "Fluid Mechanics and Thermodynamics of Turbomachinery", Seventh Edition. Amsterdam ; Boston: Butterworth-Heinemann Is an Imprint of Elsevier, 2014.

[2] Eriksson S., Bernhoff H., Leijon M., Evaluation of Different Turbine Concepts for Wind Power, *Renewable and Sustainable Energy Reviews*, **12(5)**: 1419–1434 (2008).

[3] Maleki A., Pourfayaz F., Optimal Sizing of Autonomous Hybrid Photovoltaic/Wind/Battery Power System with LPSP Technology by Using Evolutionary Algorithms, *Solar Energy*, **115**: 471–483 (2015).

[4] Khudri Johari M., Azim M., Jalil A., Faizal Mohd Shariff M., Comparison of Horizontal Axis Wind Turbine (HAWT) and Vertical Axis Wind Turbine (VAWT), *IJET*, **7(4.13)**: 74 (2018).

[5] Pinar Pérez J.M., García Márquez F.P., Tobias A., Papaelias M., Wind Turbine Reliability Analysis, *Renewable and Sustainable Energy Reviews*, **23**: 463–472 (2013).

[6] Abo-Khalil A. G., et al., Design of State Feedback Current Controller for Fast Synchronization of DFIG in Wind Power Generation Systems, *Energies*, **12(12)**: 2427 (2019).

[7] Sagharichi A., Zamani M., Ghasemi A., Effect of Solidity on the Performance of Variable-Pitch Vertical Axis Wind Turbine, *Energy*, **161**: 753–775 (2018).

[8] Aslam Bhutta M.M., Hayat N., Farooq A.U., Ali Z., Jamil Sh. R., Hussain Z., Vertical Axis wind Turbine – A Review of Various Configurations and Design Techniques, *Renewable and Sustainable Energy Reviews*, **16(4)**: 1926–1939 (2012).

[9] Kumar R., Raahemifar K., Fung A.S., A Critical Review of Vertical Axis Wind Turbines for Urban Applications, *Renewable and Sustainable Energy Reviews*, **89**: 281–291.

[10] Zamre P., Lutz T., Computational-Fluid-Dynamics Analysis of a Darrieus Vertical-Axis Wind Turbine Installation on the Rooftop of Buildings Under Turbulent-Inflow Conditions, **17**: (2022)

[11] Nazarieh M., Kariman H., S Hoseinzadeh., Numerical Simulation of Fluid Dynamic Performance of Turbulent Flow over Hunter Turbine with Variable Angle of Blades, *HFF*, Aug. 2022.

[12] Tju W., Darrieus Vertical Axis wind Turbine for Power Generation II: Challenges in HAWT and the Opportunity of Multi-Megawatt Darrieus VAWT Development, *Renewable Energy*, 12 (2015).

[13] Jin X., Zhao G., Gao K., Ju W., Darrieus Vertical Axis Wind Turbine: Basic Research Methods, *Renewable and Sustainable Energy Reviews*, **42**: 212–225 (2015).

[14] Akhlaghi M. Ghafoorian F., The Investigation of Arc Angle Rotor Blade Variations Effect of the Savonius Vertical Axis Wind Turbine on the Power and Torque Coefficients, Using 3D Modeling, *Renewable Energy Research and Applications*, (2022).

[15] Mohan Kumar P., Sivalingam K., Lim T.-C., Ramakrishna S., Wei H., Review on the Evolution of Darrieus Vertical Axis Wind Turbine: Large Wind Turbines, *Clean Technol.*, **1(1)**: 205–223 (2019)

[16] Singh M.A., Biswas A., Misra R.D., Investigation of Self-Starting and High Rotor Solidity on the Performance of a Three S1210 Blade H-Type Darrieus Rotor, *Renewable Energy*, **76**: 381–387 (2015).

[17] Lanzafame R., Mauro S., Messina M., 2D CFD Modeling of H-Darrieus Wind Turbines Using a Transition Turbulence Model, *Energy Procedia*, **45**: 131–140 (201).

[18] Qamar S.B,. Janajreh I., A Comprehensive Analysis of Solidity for Cambered Darrieus VAWTs," *International Journal of Hydrogen Energy*, **42(30)**:19420–19431 (2017).

[19] Dol S.S., Khamis A., Abdallftah M.T., Fares M., Shahid S., CFD Analysis of Vertical Axis Wind Turbine with Winglets, **3(1)**: 9 (2022).

[20] Sabaeifard P., Razzaghi H., Forouzandeh A., Determination of Vertical Axis Wind Turbines Optimal Configuration through CFD Simulations, 5.

[21] Lam H.F., Peng H.Y., Study of Wake Characteristics of a Vertical Axis Wind Turbine by Two- and Three-Dimensional Computational Fluid Dynamics Simulations, *Renewable Energy*, **90**: 386–398 (2016).

[22] Ghasemian M., Ashrafi Z.N., Sedaghat A., A Review on Computational Fluid Dynamic Simulation Techniques for Darrieus Vertical Axis Wind Turbines, *Energy Conversion and Management*, **149**: 87–100 (2017).

[23] Mohamed M.H., Performance Investigation of H-Rotor Darrieus Turbine with New Airfoil Shapes, *Energy*, **47(1)**: 522–530, (2012)

[24] Mohamed M. H., CFD Analysis for H-Rotor Darrieus Turbine as A Low Speed Wind Energy Converter, 13(2014).

[25] Yousefi Roshan M., Khaleghinia J., Eshagh Nimvari M., Salarian H., Performance Improvement of Darrieus Wind Turbine Using Different Cavity Layouts, *Energy Conversion and Management*, **246**: 114693 (2021).

[26] Paraschivoiu I., Trifu O., Saeed F., "H-Darrieus Wind Turbine with Blade Pitch Control," *International Journal of Rotating Machinery*, **2009**: 1–7 (2009)

[27] Korprasertsak N., Leephakpreeda T., CFD-Based Power Analysis on Low Speed Vertical Axis Wind Turbines with Wind Boosters, *Energy Procedia*, **79**: 963–968 (2015).

[28] Akhlagi M., Ghafoorian F., Mehrpooya M., Sharifi Rizi M., Effective Parameters Optimization of a Small Scale Gorlov Wind Turbine, Using CFD Method, *Iranian Journal of Chemistry and Chemical Engineering. (IJCCE)*, **42(7):** 2286-2304 (2022).

[29] Divakaran U. Kishore Velamati R., Ramesh A., Effect of Wind Speed on the Performance of Troposkein Vertical Axis Wind Turbine, *I.J.R.E.R.*, **9(3)**: (2019)

[30] Ghiasi P., Najafi G., Ghobadian B., Jafari A., Mazlan M., Analytical Study of the Impact of Solidity, Chord Length, Number of Blades, Aspect Ratio and Airfoil Type on H-Rotor Darrieus Wind Turbine Performance at Low Reynolds Number, *Sustainability*, **14(5)**: 2623 (2022).

[31] Gosselin R., Dumas G., Boudreau M., Parametric Study of H-Darrieus Vertical-Axis Turbines Using CFD Simulations, *Journal of Renewable and Sustainable Energy*, **8(5)**: 053301, 2016.

[32] Chong W.-T., et al., Cross Axis Wind Turbine: Pushing the Limit of Wind Turbine Technology with Complementary Design, *Applied Energy*, **207**: 78–95 (2017).

[33] Arpino F., Cortellessa G., Dell'Isola M., Scungio M., Focanti V., Rotondi M., CFD Simulations of Power Coefficients for an Innovative Darrieus Style Vertical Axis wind Turbine with Auxiliary Straight Blades, *Journal of Physics*, 9.

[34] Hoseinzadeh S., A Detailed Experimental Airfoil Performance Investigation Using an Equipped Wind Tunnel, *Flow Measurement and Instrumentation*, **6**: (2020).

[35] Hoseinzadeh S., Sohani A., Heyns S., Comprehensive Analysis of the Effect of Air Injection on the Wake Development of an Airfoil, *Ocean Engineering*, **220**: 108455 (2021).

[36] Bahrami A., Hoseinzadeh S., Heyns P.S., Mirhosseini S.M., Experimental Investigation of Co-Flow Jet's Airfoil Flow Control by Hot Wire Anemometer, *Review of Scientific Instruments*, **90(12)**: 125107 (2019)

[37] Lee Y.-T. Lim H.-C., Numerical study of the Aerodynamic Performance of a 500 W Darrieus-Type Vertical-Axis Wind Turbine, *Renewable Energy*, **9**: (2015).

[38] Hosseinkhani A., Sanaye S., Performance Prediction of a SANDIA 17-m Vertical Axis Wind Turbine Using Improved Double Multiple Streamtube, **14(12)**: 5 (2020).

[39] Chen Y., et al., A Shape Optimization of ϕ-Shape Darrieus Wind Turbine under a Given Range of Inlet Wind Speed, *Renewable Energy*, **159**: 286–299 (2020).

[40] Moghimi M. Motawej H., Developed DMST Model for Performance Analysis and Parametric Evaluation of Gorlov Vertical Axis Wind Turbines, *Sustainable Energy Technologies and Assessments*, **37**: 100616 (2020)

[41] Sharma R. Patel B., Design and Simulation of Darrieus (Eggbeater) Type Vertical Axis Wind Turbine using Open Source Software Q Blade, **1(12)**: 9.

[42] Moghimi M. Motawej H., Investigation of Effective Parameters on Gorlov Vertical Axis Wind Turbine, *Fluid Dyn*, **55(3)**: 345–363 (2020)

[43] He J., et al., CFD Modeling of Varying Complexity for Aerodynamic Analysis of H-Vertical Axis wind turbines, *Renewable Energy*, **145**: 2658–2670 (2020)

[44] Hoseinzadeh S., Garcia D.A., Numerical Analysis of Thermal, Fluid, and Electrical Performance of a Photovoltaic Thermal Collector at New Micro-Channels Geometry, *Journal of Energy Resources Technology*, **144 (6)**: 062105 (2022)

[45] Jordaan H., Stephan Heyns P., Hoseinzadeh S., Numerical Development of a Coupled One-Dimensional/Three-Dimensional Computational Fluid Dynamics Method for Thermal Analysis With Flow Maldistribution, *Journal of Thermal Science and Engineering Applications*, **13(4)**: 041017 (2021)

[46] Edwards J., Durrani N., R Howell., Qin N., "Wind Tunnel and Numerical Study of a Small Vertical Axis Wind Turbine", in *46th AIAA Aerospace Sciences Meeting and Exhibit*, Reno, Nevada, (2008)

[47] Alaimo A., Esposito A., Messineo A., Orlando C., Tumino D., 3D CFD Analysis of a Vertical Axis Wind Turbine, *Energies*, **8(4)**: 3013–3033 (2015).

[48] Ma N. et al., Airfoil Optimization to Improve Power Performance of a High-Solidity Vertical Axis Wind Turbine at a Moderate Tip Speed Ratio, *Energy*, **150**: 236–252 (2018)

[49] Bourguet R., Martinat G., Harran G., Braza M., Aerodynamic Multi-Criteria Shape Optimization of VAWT Blade Profile by Viscous Approach, in *Wind Energy*, J. Peinke, P. Schaumann, and S. Barth, Eds. Berlin, Heidelberg: Springer Berlin Heidelberg, 215–219 (2007).

[50] Lim Y.C., Chong W.T., Hsiao F.B., Performance Investigation and Optimization of a Vertical Axis Wind Turbine with the Omni-Direction-Guide-Vane, *Procedia Engineering*, **67**: 59–69 (2013).

[51] Saryazdi S.M.E. Boroushaki M., 2D Numerical Simulation and Sensitive Analysis of H-Darrieus Wind Turbine, *IJRED*, **7 (1)**: 23 (2018)

[52] Zhang B., A Novel Wake Energy Reuse Method to Optimize the Layout for Savonius-Type Vertical Axis Wind Turbines, 15 (2017).

[53] Ranjbar M. H. et al., Power Enhancement of a Vertical Axis Wind Turbine Equipped with an Improved Duct, *Energies*, **14 (18)**: 5780 (2021)

[54] Raciti Castelli M., Ardizzon G., Battisti L., Benini E., Pavesi G., Modeling Strategy and Numerical Validation for a Darrieus Vertical Axis Micro-Wind Turbine, in "Volume 7: Fluid Flow, Heat Transfer and Thermal Systems", Parts A and B, Vancouver, British Columbia, Canada, (2010), 409–418.

[55] Siddiqui M.S., Rasheed A., Kvamsdal T., Tabib M., Effect of Turbulence Intensity on the Performance of an Offshore Vertical Axis Wind Turbine, *Energy Procedia*, **80**: 312–320, 2015.

[56] Stergiannis N., Lacor C., Beeck J.V., Donnelly R., CFD Modelling Approaches Against Single Wind Turbine Wake Measurements Using RANS, *J. Phys.: Conf. Ser.*, **753**: 032062,(2016)

[57] Liamis N. Lebert Y., "Implementation of a Low Reynolds k-Epsilon Turbulence Model in a 3D Navier-Stokes Solver for Turbomachinery Flows", in *31st Joint Propulsion Conference and Exhibit*, San Diego,CA,U.S.A., (1995).

[58] Nichols R.H., Turbulence Models and Their Application to Complex Flows, 214.

[59] Mao Z., Tian W., Effect of the Blade Arc Angle on the Performance of a Savonius Wind Turbine, *Advances in Mechanical Engineering*, **7(5)**: 168781401558424 (2015).

[60] Said M.S.M., Ghani J.A., Kassim M.S., Tomadi S.H., Haron C., "Comparison between Taguchi Method and Response Surface Methodology (RSM) in Optimizing Machining Condition", *Proceeding of 1st International Conference on Robust Quality Engineering*, (2013).